FreeScatter: Enabling Concurrent Backscatter Communication Using Antenna Arrays

Qianyi Huang, Guochao Song, Wei Wang, *Senior Member, IEEE*, Huixin Dong, Jin Zhang, *Member, IEEE*, and Qian Zhang, *Fellow, IEEE*

***Abstract*—The design paradigm for backscatter tags is to avoid complex functionality and make tags as simple as possible. However, such a design principle leads to the prevalence of signal collision as tags cannot sense other tags' ongoing transmissions. The high probability of tag collision will result in low overall throughput. Although there are some existing efforts to resolve tag collisions, they either require good channel conditions or can only resolve a limited number of tags as channel capacity is deficient when SNR is low. In this article, to overcome this limitation, we bring in antenna arrays to boost the channel capacity. We propose FreeScatter, which can support scalable concurrent backscatter transmission using an antenna array. FreeScatter extracts the path that signals traveled and formulates the tags' channel coefficient using the path representations. FreeScatter further exploits the frequency agnostic property so that it can support more spatial streams than the number of antennas. The experimental results show that we can enable up to 20 tags transmitting concurrently. With the ubiquitous connectivity of battery-free tags in the near future, FreeScatter can significantly boost the network throughput.**

***Index Terms*—Antenna arrays, array signal processing, backscatter, parallel communication.**

I. Introduction

BACKSCATTER communication is an ultralow-power communication paradigm, consuming several microwatts of power [1], [2]. With backscatter communication, millions of low power, or even battery-free devices can be connected to the Internet. With this ubiquitous connectivity, a number of interesting applications are blooming, such as tracking millions of objects in the warehouse [3], [4], enabling bus stops in a smart city to broadcast messages [5] and even communication with *in-vivo* sensors implanted in deep body tissues [6]. Given this ubiquitous connectivity, medium access control becomes a bottleneck. To make the situation worse, tags are low-end devices (5–10 cents for an RFID tag) and have extremely simple circuits, which make them unable to sense other tags' ongoing transmissions in the air.

Althoug there are several existing approaches to enable a concurrent transmission in backscatter networks, they have some drawbacks. Buzz [7] incurs extra overheads as tags need to transmit multiple times in the rateless protocol. BiGroup [8] and Laissez-Faire [9] require moderate to high SNRs [10], as they rely on detecting rising and falling edges, which may be easily overwhelmed by the noise. FlipTracer [11] enables parallel decoding in hostile channel conditions. However, it can only support up to five concurrent transmitting tags as the complexity is exponential to the number of tags. The fundamental reason for this limitation is that channel capacity is limited in low SNR scenarios and is insufficient to support multiple concurrent data streams. In order to support more concurrent transmitting tags, we need to find a way to increase the channel capacity.

Nowadays, 802.11ac/11ax access points and 4G/5G base stations are equipped with multiple antennas. With multiple antennas, we have the opportunity to significantly increase the channel capacity. Unfortunately, this opportunity is not fully exploited in backscatter communication. In this article, we want to explore this opportunity to boost the throughput of backscatter networks.

Although the idea sounds straightforward, it is not easy to achieve this goal. There are two challenges need to be tackled. The first challenge is how to apply multiple antenna techniques in backscatter networks. Existing MU-MIMO techniques require the channel coefficients of each individual tag to decode the collided signals. The receiver needs to measure the channel coefficient for each tag separately. It will incur extra coordination overheads, especially when the number of tags is large. We address this challenge by formulating tags' channel coefficients using their physical locations, i.e., Angle of Arrivals (AoA) and distances. As antenna arrays can separate spatial streams [12], [13], we can obtain these geometric parameters from collided signals and thus obtain the channel coefficient for each tag. With this information, the receiver can recover each tag's data stream from the collided signals.

Manuscript received October 19, 2019; revised February 29, 2020; accepted March 19, 2020. Date of publication April 1, 2020; date of current version August 12, 2020. This work was supported in part by RGC under Contract CERG 16204418, Contract FP909, and Contract R8015; in part by the National Natural Science Foundations of China under Grant 61872420; in part by the Guangdong Key Research and Development Program under Grant 2019B121204009; in part by the Guangdong Natural Science Foundation under Grant 2017A030312008; and in part by the Project of "PCL Future Greater-Bay Area Network Facilities for Large-Scale Experiments and Applications" under Grant LZC0019. *(Corresponding author: Qian Zhang.)*

Qianyi Huang is with the Institute of Future Networks, Southern University of Science and Technology, Shenzhen 518055, China, and also with the Network Communication Research Center, Peng Cheng Laboratory, Shenzhen 518066, China (e-mail: huangqy@sustc.edu.cn).

Guochao Song, Wei Wang, and Huixin Dong are with the School of Electronic Information and Communications, Huazhong University of Science and Technology, Wuhan 430074, China (e-mail: sgc@hust.edu.cn; weiwangw@hust.edu.cn; huixin@hust.edu.cn).

Jin Zhang is with the Department of Computer Science and Engineering, Southern University of Science and Technology, Shenzhen 518055, China (e-mail: zhang.j4@sustc.edu.cn).

Qian Zhang is with the Department of Computer Science and Engineering, Hong Kong University of Science and Technology, Hong Kong (e-mail: qianzh@cs.ust.hk).

Digital Object Identifier 10.1109/JIOT.2020.2984877

Second, in multiple antenna systems, it is required that the number of concurrent communication links is no more than the number of receiving antennas [14]. That is, if we have N antennas, there could be at most N tags transmitting simultaneously. As there will be ubiquitous connectivity, it is not practical to have a large antenna array on the same scale as the number of tags. We leverage the frequency agnostic property of backscatter communication to tackle this challenge [4]. As backscatter communication works by modulating the existing radio-frequency (RF) signals in the air, its working frequency is dependent on the incident waves. By changing the frequency of the incident wave, we can have tags working at different bands. Thus, in addition to spatial domain diversity, we have frequency-domain diversity. By combining the spatial domain and frequency-domain diversity, we can overcome the limitation of antenna numbers.

In this article, we propose *FreeScatter*. *FreeScatter* explores the opportunity of multiple antennas at the receiver side and enables scalable parallel decoding for concurrent backscatter uplinks. We leave tags as simple as possible and push the decoding complexity to the receiver side. Tags with data in the transmission buffer will start sending the uplink data freely and the receiving antenna array will perform parallel decoding.

We implement *FreeScatter* on USRP software-defined radios with a 4-antenna linear array. We conduct extensive experiments to test the performance of *FreeScatter*. The experimental results show that we can enable up to 20 tags transmitting concurrently.

We summarize our contributions as follows.

1) We explore the multiple antenna opportunity in backscatter networks. We bring in antenna arrays to boost the throughput in backscatter networks.
2) We propose and design *FreeScatter*, which enables scalable parallel decoding by combining the spatial domain and frequency-domain diversity, overcoming the limitation of antenna numbers.
3) We conduct extensive experiments to test the performance of *FreeScatter*. Results show that *FreeScatter* works robustly in low SNR scenarios and can support up to 20 tags transmitting concurrently.

II. Related Works

In this section, we review related works from two aspects: 1) backscatter communication and 2) multiple access control in backscatter communication.

A. Backscatter Communication

Backscatter communication is a passive communication paradigm. It works by modulating the existing RF signals in the air. RFID [3], [4] is a well-established backscatter technique. With an RFID reader, battery-free RFID tags can harvest energy from the reader's RF signals and respond to the reader's query. Besides RFID, ambient backscatter communication emerges as a popular communication method for low-end devices. Instead of relying on a dedicated reader, tags can modulate ambient RF signals in the air, such as TV [1], Wi-Fi [15], and FM signals [5]. MOXScatter [16] enables backscatter tags to modulate Wi-Fi spatial streams while keeping the ongoing Wi-Fi transmissions unaffected. Recent work has greatly extended the communication range of ambient backscatter to 3 km [17], [18], which makes ambient backscatter practical for city-level deployment.

B. Resolving Collision for Backscatter Communication

In order to achieve ultralow-power consumption, backscatter tags use a very simple circuit design. These tags do not have the capability to sense other tags' ongoing transmissions.

Slotted Aloha: RFID employs slotted Aloha to achieve multiple access control. The reader divides time into slots and tags will randomly choose one slot to transmit. When more than one tags choose the same slot, the signals will collide and tags need to retransmit at the next round.

MAC With Coordination: The task of carrier sense could be delegated to the RF source in ambient backscatter [17], [19], where the RF source arbitrates access between multiple tags using TDMA. Besides TDMA, LoRa backscatter [17] enables multiple tags transmitting concurrently by letting tags work at different bands (i.e., FDMA) and using different spread factors (i.e., CDMA). Buzz [7] makes each tag transmit in a random subset of collisions. Leveraging the sparsity and rateless nature of the collided code, Buzz can recover tags' data from the collided signals. As the tags need to transmit multiple times in the rateless protocol, Buzz increases the tags' energy consumption. NetScatter [20], essentially a CDMA scheme, enables up to 256 LoRa backscatter nodes transmit concurrently, where it allocates orthogonal codes to each node. Zhao *et al.* [21] enabled the OFDMA scheme among backscatter nodes, which is essentially an FDMA mechanism.

Resolving Collisions Using IQ Domain: BiGroup [8], FlipTracer [11], and Hubble [22] exploit tags' IQ domain feature. When there are M tags, there will be 2^M clusters on the IQ plane. The number of clusters increases exponentially with the number of tags, and thus these methods are hard to scale. They can decode up to five concurrent tags. Based on the observation that tags' edges are interleaving in time, *Laissez-Faire* combines the temporal domain and the IQ domain feature and can support up to 16 tags transmitting concurrently. As *Laissez-Faire* relies on detecting tags' rising and falling edges, it only works in the scenarios of moderate to high SNRs, as edges may be overwhelmed by noise in low SNR scenarios [10].

Antenna Arrays for Parallel Decoding: Previous work has also adopted signal separation techniques to enable parallel decoding for backscatter communication using antenna arrays [14]. The limitation is that given N antennas, they can decode N tags in parallel. As it is hard to scale the number of antennas in practice, existing methods are not practical given the ubiquitous connectivity of nodes in the near future. To overcome this limitation, *FreeScatter* adds frequency-domain diversity by leveraging the frequency agnostic property of backscatter communication, and thus *FreeScatter* can decode more than N tags concurrently.

III. Bring Multiple Antennas Into Backscatter Networks

In this section, we first explore the opportunity of antenna arrays in backscatter networks and then discuss the frequency agnostic property.

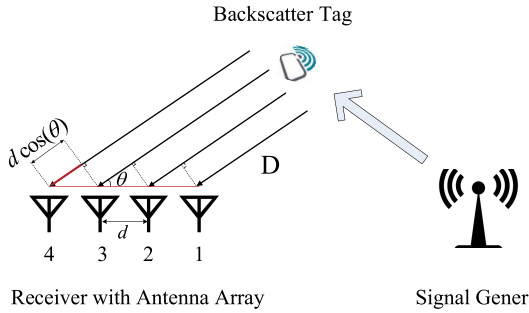

Fig. 1. Linear array with four antennas. Consider a signal from angle θ. It travels a distance D to reach the first antenna and travels an additional path $dcos(\theta)$ to reach the second antenna.

A. Backscatter Communication and Multiple Access Control

Backscatter communication utilizes ambient RF signals in the air. By switching its antenna in absorbing or reflecting states, a backscatter tag can modulate ambient RF signals. In this way, it can send information without active radio wave transmission. Thus, it consumes almost zero energy, usually about several microwatts. The ambient signals can come from ongoing transmissions in the air, such as TV [1] and FM signals [5]. There could also be a dedicated signal generator, such as an RFID reader or a signal helper [19].

Multiple access control in backscatter communication remains an opening issue [23]. Due to the minimalist design paradigm, tags do not have the capability to sense other tags' ongoing transmissions. Although there are some existing works enabling parallel decoding in backscatter networks, their main idea is to leverage the asymmetric capability between the receiver and the low-end tags [8], [9], [11]. The receiver is a powerful device with a high sampling rate (e.g., up to 25 Mb/s) while tags are transmitting at low rates (e.g., 100 kb/s). Thus, the receiver has the capability to decode multiple concurrent transmitting tags. However, when in hostile conditions, edge transitions will be overwhelmed by noise, leading to a decoding failure. Furthermore, in these IQ-cluster-based methods (e.g., [8], [9], [11], and [22]), the number of clusters is exponential to the number of tags, restricting the maximum number of decodable tags. We need to find a way to support scalable parallel decoding.

B. Antenna Arrays for Parallel Decoding

Nowadays, 802.11ac/11ax access points and 4G/5G cellular base stations are equipped with multiple antennas. Multiple antennas bring the opportunity to significantly boost the channel capacity. Thus, we bring antenna arrays into backscatter networks to enable scalable parallel decoding.

Here, we consider the linear array. As shown in Fig. 1, a signal from angle θ propagates a distance D and reaches the first antenna. As antennas are separated by d, the signal propagates an additional path $d\cos\theta$ to reach the second antenna. That is, signals are delayed by an additional phase $[(2\pi d\cos\theta)/\lambda]$, where d is the distance between antennas and λ is the wavelength. Given N antennas, we can write the received signals as

$$\begin{bmatrix} R_1 \\ R_2 \\ \cdots \\ R_N \end{bmatrix} = Ae^{-j2\pi\phi} \begin{bmatrix} 1 \\ e^{-j2\pi\frac{d\cos\theta}{\lambda}} \\ \cdots \\ e^{-j2\pi\frac{(N-1)d\cos\theta}{\lambda}} \end{bmatrix} s(t) = A\vec{\alpha}(D,\theta)s(t) \quad (1)$$

where A represents signal attenuation, $\vec{\alpha}(D,\theta)$ is the steering vector, and $s(t)$ is the data transmitted by the tag. In this way, we formulate the channel coefficient for a tag using its geometric parameters. When there are M tags, the received signals can be written as

$$\mathbf{R} = \mathbf{H}\cdot\mathbf{S} = \left[A_1\vec{\alpha}(D_1,\theta_1),\ldots,A_M\vec{\alpha}(D_M,\theta_M)\right]\begin{bmatrix} s_1(t) \\ s_2(t) \\ \cdots \\ s_M(t) \end{bmatrix}. \quad (2)$$

Here, $\mathbf{H}$ is the $N \times M$ channel matrix. We will discuss how to obtain the parameters A_i, D_i, and θ_i in Section IV. With $\mathbf{H}$, we can decode tags' data streams by

$$\mathbf{S} = \mathbf{H}^{-1}\mathbf{R}. \quad (3)$$

For (3) to hold, it requires that $N \geq M$. It indicates that for an antenna array with N antennas, it can support at most N tags transmitting concurrently. However, the number of tags is usually larger than the number of antennas. In order to support scalable parallel decoding, we need to have a very large antenna array, which is not feasible in practice.

C. Frequency Agnostic Property of Backscatter Communication

As we introduced in Section II-A, backscatter is a passive communication paradigm, where tags send data by modulating existing RF signals in the air. When we change the frequency of the ambient signals, tags will be working on different bands. Ma *et al.* [4] demonstrated that RFID tags are responsive over a bandwidth of 300 MHz.

Based on this observation, we can add frequency-domain diversity into decoding. By changing the frequency of the carrier wave, we are actually changing the value of λ in (1). If we use k frequencies, the steering vector $\alpha(D,\theta)$ can be rewritten as

$$\vec{\alpha}(D,\theta) = \left[e^{-j2\pi\frac{D}{\lambda_1}}, e^{-j2\pi\frac{D+d\cos\theta}{\lambda_1}}, \ldots, e^{-j2\pi\frac{D+(N-1)d\cos\theta}{\lambda_1}}, \ldots, e^{-j2\pi\frac{D+(N-2)d\cos\theta}{\lambda_k}}, e^{-j2\pi\frac{D+(N-1)d\cos\theta}{\lambda_k}}\right]^T. \quad (4)$$

In this way, we actually increase the number of rows in $\mathbf{H}$ to $k \times N$, without increasing the number of columns (i.e., M, given M tags). In this way, we can overcome the limitation of antenna number and enable scalable parallel decoding.

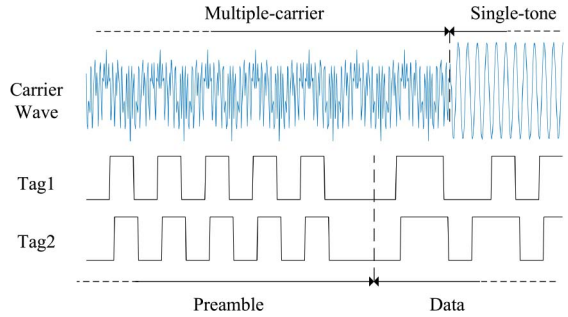

Fig. 2. Signal generator first generates a multiple carrier wave, followed by a single-tone constant wave. The multiple carrier wave covers the tags' preamble.

IV. FreeScatter

In this section, we present the design details of *FreeScatter*. We first present how we incorporate the frequency diversity in backscatter communication and then discuss how we decode tags' data streams from collided signals.

A. Incorporating Frequency Diversity by Multiple Carrier Preamble

When the signal generator starts transmitting radio waves, the radio waves will charge the capacitor on the tags and the tags will start backscatter communication. In *FreeScatter*, the signals from the signal generator consist of two parts: 1) the multiple carrier part and 2) the single-tone part, as shown in Fig. 2. The single-tone part is for tags to transmit data. We use a single-tone wave because harvesting energy from the single-tone wave is more efficient, which is critical for battery-free tags. The multiple carrier part is for tags to transmit preambles.

The relative response delay of RFID tags is about several microseconds [8]. Assuming that tags are transmitting at 100 kb/s, the delay is less than one-bit duration. This delay is much shorter than the duration of the preamble, which can be neglected. When tags detect the presence of the carrier wave, they will start backscatter the multiple carrier signals as their preambles. In this way, the backscattered signals from the tags also contain two parts: 1) the multiple carrier part, corresponding to tags' preamble and 2) the single-tone part, containing tags' data. Below, we describe how we obtain the channel matrix $\mathbf{H}$ from the multiple carrier preamble.

Step 1 (Determining D_i and θ_i): We adopt SpotFi [13] to determine the parameters D_i and θ_i in $\mathbf{H}$. From the multiple carrier preamble part, we can construct a smoothed CSI matrix as in [13]. Given four antennas and 26 subcarriers, we use a 2×16 subarray to form a 32-element vector and we can find 33 such subarrays from the original 4×26 CSI matrix, i.e., $(4-2+1)\times(26-16+1) = 33$. Thus, the constructed smoothed CSI matrix $\mathbf{x}$ is of dimension 32×33. It means that we can separate up to 32 signal sources simultaneously.

By the MUSIC algorithm [12], [13], [24], the correlation matrix $\mathbf{R}_{xx} = \mathbb{E}[\mathbf{x}\mathbf{x}^*]$ has E eigenvalues associated with E eigenvectors. The k eigenvectors with nonzero eigenvalues, denoted by $\mathbf{E_k}$, represent k incoming signals and the remaining $E - k$ eigenvectors, denoted by $\mathbf{E_n}$, represent the noise subspace. The signal subspace is orthogonal to the noise subspace.

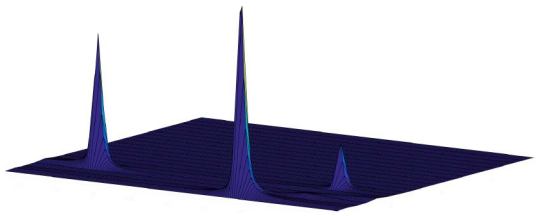

Fig. 3. On the AoA-ToF power spectrum, there are three peaks. Each one corresponds to a tag.

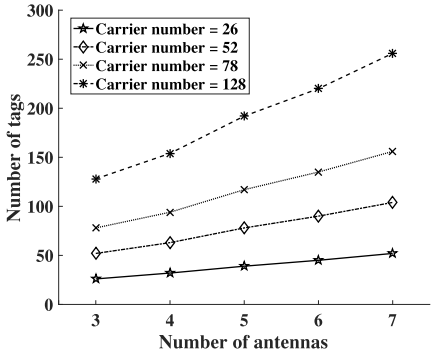

Fig. 4. Number of tags that *FreeScatter* can decode in parallel. It increases with the number of antennas and subcarriers.

We can determine tags' parameter θ_i's and D_i's by finding the steering vector $\alpha(D_i, \theta_i)$'s that is orthogonal to the noise subspace

$$P(D, \theta) = \frac{1}{\vec{\alpha}(D, \theta)\mathbf{E_N}\mathbf{E_N^*}\vec{\alpha}(D, \theta)} \tag{5}$$

will yield a sharp peak at signals' arriving angle θ and distance D. Fig. 3 shows an example of the AoA-ToF spectrum with three tags. Due to space limitations, interested readers may refer to [13] for the details.

Step 2 (Determining A_i): After determining D_i and θ_i, (2) becomes a set of linear equations with A_i's as unknown variables. We can solve these linear equations to get the values of A_i's.

The number of collided signals that *FreeScatter* can separate depends both on the number of antennas and subcarriers. Fig. 4 shows the number of concurrent uplinks that *FreeScatter* can support with different numbers of antennas and subcarriers. As the number of antennas is usually limited, to enable scalable parallel decoding, *FreeScatter* can use a large bandwidth and increase the number of subcarriers.

B. Decode the Collided Signals

To improve tags' energy harvesting efficiency, *FreeScatter* uses the single-tone carrier wave for the data part. As we can see from (1), with the single-tone carrier wave, the channel matrix $\mathbf{H}$ is of dimension $N \times M$, where N is the number of antennas and M is the number of collided tags. When there are more tags than antennas, we cannot directly apply (3) to obtain tags' data.

A good thing for backscatter communication is that tags simply switch between two states to modulate ambient signals. The tag could either be in the absorbing state or the reflecting

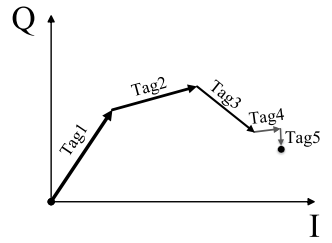

Fig. 5. Received signal is a weighted summation of signals from all tags. Tags with large signal amplitudes have heavier weights, i.e., Tags 1–3, while Tags 4 and 5 with small signal amplitudes have lighter weights.

state. Thus, given M tags, there are 2^M possible combinations. When M is small, it is possible to iterate over all the possible combinations to find the one with maximum likelihood. However, the search domain increases exponentially with the number of tags. When M increases to 20, the size of the search domain is at an order of 10^6. It becomes infeasible to iterate the whole search domain.

We observe that we can decouple the search domain according to tags' signal qualities. The received signals are the summation of signals from all tags, as shown in Fig. 5.

We can write it as

$$\mathbf{R} = \sum_{i=1}^{M} A_i \vec{\alpha}(D_i, \theta_i) s_i(t) \tag{6}$$

where A_i determines the amplitude of the signal and $\vec{\alpha}(D_i, \theta_i)$ determines the phase. We can consider $\mathbf{R}$ as the weighted summation of tags' signals, where tags with large signal amplitudes have heavier weights whereas tags with small amplitudes have lighter weights.

We sort A_i in the decreasing order and find the index j s.t. $A_j > \sum_{i=j+1}^{M} A_i$. $\mathbf{R}$ can be decomposed into two parts

$$\mathbf{R} = \sum_{i=1}^{j} A_i \vec{\alpha}(D_i, \theta_i) s_i(t) + \sum_{i=j+1}^{M} A_i \vec{\alpha}(D_i, \theta_i) s_i(t). \tag{7}$$

The search domain could also be decomposed into two parts accordingly, S_1 and S_2, where $\|S_1\| = 2^j$ and $\|S_2\| = 2^{M-j}$. We can first search among S_1 to determine the first part in (7). After fixing on the first part, *FreeScatter* continues to search in S_2 for the second part. This is reasonable because the value of the second part in (7) could hardly change the search results for the first part.

In this way, we effectively reduce the size of the search domain from 2^M to $2^j + 2^{M-j}$. Consider the case when there are 20 tags and $j = 12$, we reduce the size of the search domain by 240 times. The details can be found in Algorithm 1. For the ease of expression, we define $\vec{s}_1(t) = [s_1(t), s_2(t), \ldots, s_j(t)]$ and $\vec{s}_2(t) = [s_{j+1}(t), s_{j+2}(t), \ldots, s_M(t)]$.

Algorithm 1 Decoding Collided Signals

```
A_i ← sort(A_i, "descending")
Find j s.t. A_j > Σ_{l=j+1}^{M} A_l.
for t ← 1, ..., l do
    for p ← 1, ..., 2^j do                ▷ Search for the first part
        s⃗_1(t) ← S_1(p).
        E_1(p) = R(t) − Σ_{i=1}^{j} A_i α⃗(D_i, θ_i) s_i(t)
    end for
    s⃗_1(t) ← argmin_{s⃗_1(t)} E_1.
    for p ← 1, ..., 2^{M−j} do ▷ Search for the second part
        s⃗_2(t) ← S_2(p).
        E_2(p) = min(E_1) − Σ_{i=j+1}^{M} A_i α⃗(D_i, θ_i) s_i(t).
    end for
    s⃗_2(t) ← argmin_{s⃗_2(t)} E_2.
end for
```

V. Implementation

In this section, we describe our experimental setup.

Signal Generator: We use Keysight MXG Vector Signal Generator N5182B as the signal helper. Its output power is set to be +18 dBm. The RF output port is connected to a 3-dBi VERT 2450 antenna. It is working at 2.4 GHz. For the multiple carrier wave part, it generates a 120-MHz carrier wave with 64 subcarriers, among which 52 subcarriers are active. We obtain a CSI value every two subcarriers, resulting in 26 CSI values, each separated by 3.75 MHz. For the single-tone part, it generates the 2.4-GHz constant wave.

Receiver: We use two NI USRP-2943R software-defined radios to form a 4-antenna receiver. Each USRP has two RF ports and two USRPs are synchronized by an external clock. We calibrate the phase offset among different antenna ports using the methods proposed in [25]. The four antennas are arranged on a line to form a linear array. There is a 6 cm separation among antennas. The sampling rate is set to be 120 MHz. To prevent the carrier frequency offset, we also let the signal generator and the receiver share the same clock.

Backscatter Tag: We design the tags according to [26] and [27]. The data rate for each tag is 100 kb/s.

VI. Experimental Results

In this section, we present the evaluation results. We first show the effects of AoA and distance estimation errors on decoding performance. After that, we show that *FreeScatter* can greatly reduce maximum-likelihood decoding latency. Finally, we show the overall network throughput.

A. BER With Inaccurate AoA and Distance Estimation

Errors in estimating AoA and distance can lead to inaccurate channel matrix $\mathbf{H}$, which will harm the decoding performance. Here, we show that how inaccurate AoA and distance estimation will affect bit error rates.

Fig. 6 shows that BER increases with errors in AoA estimation. When the AoA error is less than 10°, the BERs are less than 0.003. When the errors in the AoA estimation increase, BERs increase dramatically. In the case with eight tags, BER increases to be above 0.025 when AoA error is above 15°. Similar is the case for distance estimation, as shown in Fig. 7. When the error in distance estimation is less than 10 cm, BERs are less than 0.008. When the error increases to 20 cm, BER increases to be above 0.11.

It indicates that *FreeScatter* relies on the accurate estimation of AoA and distance. Given that there are a number

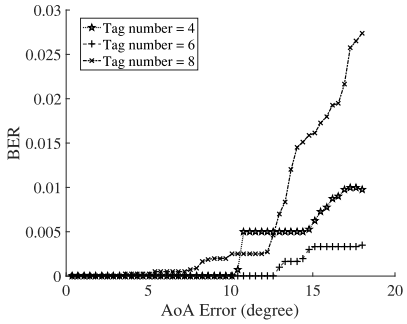

Fig. 6. Effect of AoA errors on BER.

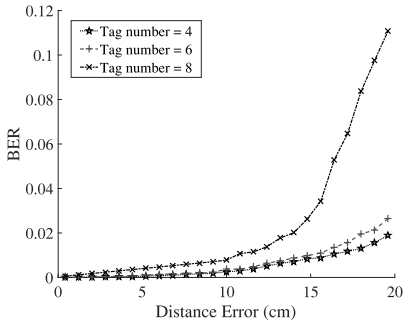

Fig. 7. Effect of distance errors on BER.

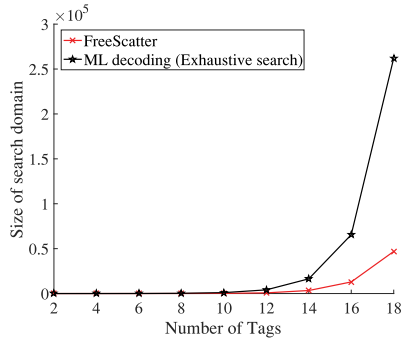

Fig. 8. Complexity comparison.

of works on localizing backscatter tags, which can achieve subcentimeter accuracy [4], [28], we believe that we can get highly accurate AoA and distance, and the effect of AoA and distance estimation errors on decoding performance can be neglected. As accurate localization of backscatter tags is not in the scope of this article, here, we do not discuss how to improve AoA and distance estimation accuracy.

B. Maximum-Likelihood Decoding With SNR-Based Pruning

FreeScatter prunes the search domain during maximum-likelihood decoding based on tags' signal qualities. Here, we compare the decoding complexity and BER between *FreeScatter* and the exhaustive search method. From Fig. 8, we can see that when there are above 16 tags, *FreeScatter* can greatly reduce the size of the search domain. The reason is that even when *FreeScatter* could only decouple the search domain of one tag from the other tags, it could reduce the total search space by half; if *FreeScatter* could decouple two

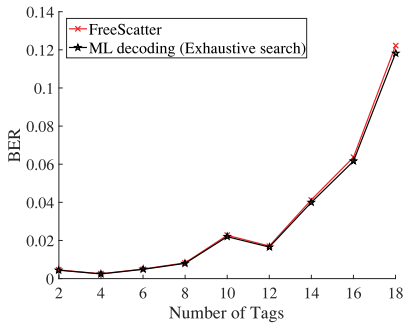

Fig. 9. BER comparison.

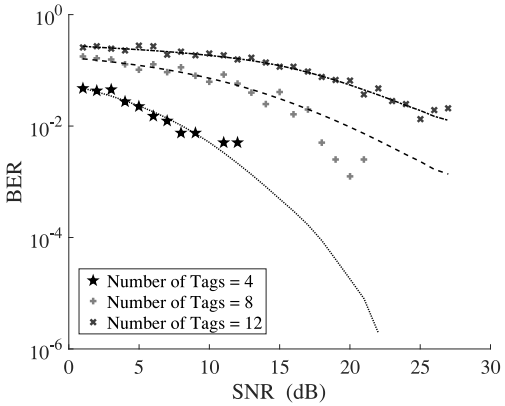

Fig. 10. Bit error rates for tags with different SNRs.

tags from the other tags, it could reduce the search domain by four times. Given that tags are separately deployed in the environment, their signal amplitudes are different as their distances to the signal generator and the receiver are different. Thus, *FreeScatter* can decouple the search domain for tags with good and poor SNRs. This reduction in decoding latency is significant especially when there are more than 12 tags.

Fig. 9 compares BER performance. Here, we show the average BERs for all tags. We can see that BERs are very close between *FreeScatter* and the exhaustive search method. It indicates that *FreeScatter* can greatly reduce decoding latency without degrading the performance.

C. Overall Performance

Fig. 10 shows the BERs under different SNRs. In order to achieve the same level of BERs, it requires a higher SNR to support a larger number of tags. This is reasonable because channel capacity increases with SNR.

Fig. 11 shows the total network throughput with an increasing number of tags. When the number of tags is less than 12, the throughput increases almost linearly with the number of tags. When there are more than 16 tags, the interference among tags leads to decoding errors. When there are 20 tags, the network throughput is 1.35 Mb/s. Although this number is smaller than the maximum throughput achieved in FlipTracer [11], we note that FlipTracer only enables five tags transmitting simultaneously, each with 500-kb/s data rate, leading to a maximum throughput approaching 2 Mb/s. However, it is hard for FlipTracer to support more concurrent

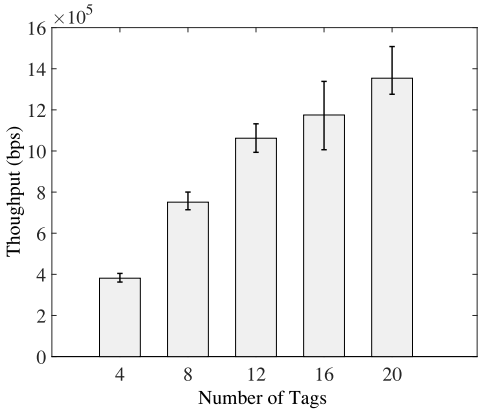

Fig. 11. Network throughput for 4, 8, 12, 16, and 20 tags.

TABLE I
PERFORMANCE COMPARISON

	Maximum Number of Decodable Tags	Required SNR @ BER<0.01
BiGroup [8]	5	$>$ 20 dB @ 4 tags
LF-Backscatter [9]	16	$>$ 10 dB @ 1 tag
FlipTracer [11]	5	N/A
FreeScatter	20	$\sim$ 7dB @ 4tags

data streams, as FlipTracer explores the constellation domain feature, where collided signals form clusters on the constellation domain. With n tags, the number of clusters on the I/Q plane is 2^n. The complexity goes exponentially with the number of colliding tags. Compared with FlipTracer, *FreeScatter* enables 20 tags transmitting concurrently, each with 100-kb/s data rate. *FreeScatter* has the merit of enabling ubiquitous connectivity in the era of smart cities, where there is a large number of nodes while each node has a small amount of traffic.

Table I compares FreeScatter with the state-of-the art solutions, in terms of maximum resolvable tags and the required SNR to achieve low BERs. We can see that FreeScatter can support more tags than BiGroup [8] and FlipTracer [11]. Compared with LF-Backscatter [9], FreeScatter can work in low SNR scenarios.

In order to support backscatter networks with more than 20 tags, *FreeScatter* can incorporate other MAC protocols, such as slotted Aloha. As it is unlikely that there will be more than 20 tags colliding in one-time slot, *FreeScatter* can greatly improve the success rate of each query.

VII. DISCUSSION

In this section, we discuss some implementation issues in *FreeScatter*.

A. Bandwidth Versus Subcarrier Number

Theoretically speaking, the number of tags that *FreeScatter* can decode in parallel is dependent on the number of antennas and subcarriers. It is independent on the bandwidth separation among subcarriers. However, in practice, when the subcarriers are closely placed among a small bandwidth, we will have

$$e^{-j2\pi\frac{D}{\lambda_1}} \approx e^{-j2\pi\frac{D}{\lambda_2}} \approx \cdots \approx e^{-j2\pi\frac{D}{\lambda_k}}.$$

In this way, we cannot determine D in a very accurate way. In order to achieve high accuracy in estimating D, we need a reasonable large bandwidth. In our implementation, we use 26 subcarriers with 3.75-MHz separation.

Ma *et al.* [4] found that tags are responsive over a bandwidth of 300 MHz. Thus, it is possible to increase the number of subcarriers by using a large bandwidth for the multiple carrier wave. As *FreeScatter* only uses the multiple carrier wave for tags' preamble, it will not occupy the whole bandwidth for long periods of time. However, the ISM band is quite limited (e.g., from 902 to 928 MHz). One workaround is to transmit with high power in the ISM band while transmitting at a low-power level outside the ISM band to be compliant with the FCC regulations as in [4]. This is not in the scope of this article and we refer interested readers to [4] for more details.

B. Tag Asynchrony Problem

It is a well-known fact that backscatter tags are unsynchronized. *FreeScatter* does not require tags to be strictly synchronized and here we discuss how *FreeScatter* handles the tag asynchrony problem.

The asynchrony problem manifests it in two aspects. First, tags start transmission with a random initial offset, i.e., the response delay. The response delay is due to a lot of factors, such as the charging characteristic of the capacitor and the placement and orientation of the tags [9]. It mainly affects the preamble part of tag transmission. FreeScatter handles this by introducing a cyclic prefix (CP) in the multiple carrier wave, which can handle the delay spread caused by the multipath channel in OFDM signals. Even though tags' data are not synchronized, as long as the relative offset is shorter than the CP, CP can effectively handle the intersymbol interference caused by tag asynchrony in the preamble part.

Second, tags' clocks are asynchronous. This will lead to offsets in tags' bit duration, about 1% for each bit [8]. This drift will accumulate over time and thus this effect becomes obvious in the data part of the packets. As FreeScatter decodes the data part using the maximum-likelihood method, it does not rely on tags' state transition to detect transitions among clusters on the IQ domain. Thus, this drift will not degrade the decoding performance.

C. Implementation Issues

In the experiment, as we generate a 120-MHz multicarrier wave, according to the Nyquist sampling theorem, we set the sampling rate of the receiver to be 120 MHz. However, such a high sampling rate is unavailable on commercial devices. In order to implement *FreeScatter* on commercial devices, we can use frequency hopping to achieve frequency-domain diversity. In this way, the receiver does not need to have high sampling rate, as the signal is a narrow-band signal while changing its center frequency over time. As this is out the scope of this article, we leave it to the future work.

VIII. CONCLUSION

In this article, we proposed *FreeScatter*. *FreeScatter* explores the multiple antenna opportunity to enable scalable

concurrent backscatter transmission. By combining the spatial domain and frequency-domain diversity, *FreeScatter* overcomes the limitation of antenna numbers in MU-MIMO and enables parallel decoding for more concurrent data streams than the number of antennas. With *FreeScatter*, backscatter tags can start transmission freely and the receiver can perform parallel decoding. The experimental results showed that *FreeScatter* can work robustly in low SNR scenarios and can support up to 20 tags transmitting simultaneously. In the near future with the ubiquitous connectivity of low-end devices in smart cities, homes, and warehouses, *FreeScatter* can significantly boost the network throughput.

REFERENCES

[1] V. Liu, A. Parks, V. Talla, S. Gollakota, D. Wetherall, and J. R. Smith, "Ambient backscatter: Wireless communication out of thin air," in *Proc. Conf. SIGCOMM*, 2013, pp. 39–50.

[2] P. Zhang, P. Hu, V. Pasikanti, and D. Ganesan, "EkhoNet: High speed ultra low-power backscatter for next generation sensors," in *Proc. 20th Annu. Int. Conf. Mobile Comput. Netw. (MobiCom)*, 2014, pp. 557–568.

[3] Y. Ma, N. Selby, and F. Adib, "Drone relays for battery-free networks," in *Proc. Conf. ACM Special Interest Group Data Commun. (SIGCOMM)*, 2017, pp. 335–347.

[4] Y. Ma, N. Selby, and F. Adib, "Minding the billions: Ultra-wideband localization for deployed RFID tags," in *Proc. 23rd Annu. Int. Conf. Mobile Comput. Netw. (MobiCom)*, 2017, pp. 248–260.

[5] A. Wang, V. Iyer, V. Talla, J. R. Smith, and S. Gollakota, "FM backscatter: Enabling connected cities and smart fabrics," in *Proc. 14th USENIX Conf. Netw. Syst. Design Implement. (NSDI)*, 2017, pp. 243–258.

[6] Y. Ma, Z. Luo, C. Steiger, G. Traverso, and F. Adib, "Enabling deep-tissue networking for miniature medical devices," in *Proc. Conf. ACM Special Interest Group Data Commun. (SIGCOMM)*, 2018, pp. 417–431.

[7] J. Wang, H. Hassanieh, D. Katabi, and P. Indyk, "Efficient and reliable low-power backscatter networks," in *Proc. ACM SIGCOMM Conf. Appl. Technol. Architect. Protocols Comput. Commun.*, 2012, pp. 61–72.

[8] J. Ou, M. Li, and Y. Zheng, "Come and be served: Parallel decoding for COTS RFID tags," in *Proc. 21st Annu. Int. Conf. Mobile Comput. Netw. (MobiCom)*, 2015, pp. 500–511.

[9] P. Hu, P. Zhang, and D. Ganesan, "Laissez-faire: Fully asymmetric backscatter communication," in *Proc. ACM Conf. SIGCOMM*, 2015, pp. 255–267.

[10] D. Katabi, "Laissez-faire: Fully asymmetric backscatter communication," in *Proc. SIGCOMM*, 2015.

[11] M. Jin, Y. He, X. Meng, Y. Zheng, D. Fang, and X. Chen, "Fliptracer: Practical parallel decoding for backscatter communication," in *Proc. 23rd Annu. Int. Conf. Mobile Comput. Netw. (MobiCom)*, 2017, pp. 275–287.

[12] J. Xiong and K. Jamieson, "ArrayTrack: A fine-grained indoor location system," in *Proc. 10th USENIX Conf. Netw. Syst. Design Implement. (NSDI)*, 2013, pp. 71–84.

[13] M. Kotaru, K. Joshi, D. Bharadia, and S. Katti, "SpotFi: Decimeter level localization using WiFi," *ACM SIGCOMM Comput. Commun. Rev.*, vol. 45, no. 4, pp. 269–282, 2015.

[14] A. F. Mindikoglu and A.-J. van der Veen, "Separation of overlapping RFID signals by antenna arrays," in *Proc. IEEE Int. Conf. Acoust. Speech Signal Process. (ICASSP)*, Las Vegas, NV, USA, 2008, pp. 2737–2740.

[15] B. Kellogg, A. Parks, S. Gollakota, J. R. Smith, and D. Wetherall, "Wi-Fi backscatter: Internet connectivity for RF-powered devices," *ACM SIGCOMM Comput. Commun. Rev.*, vol. 44, no. 4, pp. 607–618, 2015.

[16] J. Zhao, W. Gong, and J. Liu, "Spatial stream backscatter using commodity WiFi," in *Proc. 16th Annu. Int. Conf. Mobile Syst. Appl. Serv. (MobiSys)*, 2018, pp. 191–203.

[17] V. Talla, M. Hessar, B. Kellogg, A. Najafi, J. R. Smith, and S. Gollakota, "LoRa backscatter: Enabling the vision of ubiquitous connectivity," *Proc. ACM Interact. Mobile Wearable Ubiquitous Technol.*, vol. 1, no. 3, p. 105, 2017.

[18] A. Varshney, O. Harms, C. Pérez-Penichet, C. Rohner, F. Hermans, and T. Voigt, "LoRea: A backscatter architecture that achieves a long communication range," in *Proc. 15th ACM Conf. Embedded Netw. Sens. Syst. (Sensys)*, 2017, pp. 1–2.

[19] B. Kellogg, V. Talla, S. Gollakota, and J. R. Smith, "Passive Wi-Fi: Bringing low power to Wi-Fi transmissions," in *Proc. 13th USENIX Symp. Netw. Syst. Design Implement. (NSDI 16)*, 2016, pp. 151–164.

[20] M. Hessar, A. Najafi, and S. Gollakota, "Netscatter: Enabling large-scale backscatter networks," in *Proc. 16th USENIX Conf. Netw. Syst. Design Implement. (NSDI)*, 2019, pp. 271–283.

[21] R. Zhao *et al.*, "OFDMA-enabled Wi-Fi backscatter," in *Proc. 25th Annu. Int. Conf. Mobile Comput. Netw. (MobiCom)*, 2019, pp. 1–15.

[22] M. Jin, Y. He, X. Meng, D. Fang, and X. Chen, "Parallel backscatter in the wild: When burstiness and randomness play with you," in *Proc. 24th Annu. Int. Conf. Mobile Comput. Netw. (MobiCom)*, 2018, pp. 471–485.

[23] N. Van Huynh, D. T. Hoang, X. Lu, D. Niyato, P. Wang, and D. I. Kim, "Ambient backscatter communications: A contemporary survey," *IEEE Commun. Surveys Tuts.*, vol. 20, no. 4, pp. 2889–2922, 4th Quart., 2018.

[24] R. Schmidt, "Multiple emitter location and signal parameter estimation," *IEEE Trans. Antennas Propag.*, vol. 34, no. 3, pp. 276–280, Mar. 1986.

[25] M. Kotaru and S. Katti, "Position tracking for virtual reality using commodity WiFi," in *Proc. Conf. Comput. Vis. Pattern Recognit. (CVPR)*, 2017, pp. 2671–2681.

[26] V. Iyer, V. Talla, B. Kellogg, S. Gollakota, and J. Smith, "Inter-technology backscatter: Towards Internet connectivity for implanted devices," in *Proc. ACM SIGCOMM Conf.*, 2016, pp. 356–369.

[27] P. Zhang, M. Rostami, P. Hu, and D. Ganesan, "Enabling practical backscatter communication for on-body sensors," in *Proc. ACM SIGCOMM Conf.*, 2016, pp. 370–383.

[28] L. Yang, Y. Chen, X.-Y. Li, C. Xiao, M. Li, and Y. Liu, "Tagoram: Real-time tracking of mobile RFID tags to high precision using COTS devices," in *Proc. 20th Annu. Int. Conf. Mobile Comput. Netw. (MobiCom)*, 2014, pp. 237–248.

Qianyi Huang received the bachelor's degree in computer science from Shanghai Jiao Tong University, Shanghai, China, in July 2013 and the Ph.D. degree from the Department of Computer Science and Engineering, Hong Kong University of Science and Technology, Hong Kong, in November 2018.

She is a Research Assistant Professor with the Southern University of Science and Technology, Shenzhen, China. She is also affiliated with Peng Cheng Laboratory. Her research interests lie in mobile computing, Internet of Things, and security.

Guochao Song received the B.S. degree in electronic and information engineering from China University of Geosciences, Wuhan, China, in June 2015. He is currently pursuing the Ph.D. degree with the Wuhan National Laboratory for Optoelectronics, Huazhong University of Science and Technology, Wuhan.

His current research interests include distributed MIMO and backscatter communications.

Wei Wang (Senior Member, IEEE) received the Ph.D. degree from the Department of Computer Science and Engineering, Hong Kong University of Science and Technology, Hong Kong, in January 2015.

He is currently a Full Professor with the School of Electronic Information and Communications, Huazhong University of Science and Technology, Wuhan, China. He has published two books and 70 refereed papers in international leading journals and primer conferences. He is the inventor of three U.S. and 20 Chinese patents. His research interests include PHY/MAC design and mobile computing in wireless systems.

Prof. Wang won the Best Paper Award at IEEE ICC 2019. He was selected as the Young Elite Scientist Sponsorship Program, the China Association for Science and Technology, and the Hundred Talents Program, Hubei Province, China. He served on a TPC of INFOCOM, GBLOBECOM, and ICC. He served as an Editor for IEEE ACCESS, the *International Journal of Communication Systems*, and *China Communications*, and a Guest Editor for *Wireless Communications and Mobile Computing* and IEEE COMSOC MMTC Communications.

Huixin Dong received the bachelor's degree in communication engineering from Wuhan University of Technology, Wuhan, China, in July 2018. He is currently pursuing the master's degree in information and communication engineering with the Huazhong University of Science and Technology, Wuhan, under the supervision of Prof. W. Wang.

His research direction is related to the wireless technology of Internet of Things.

Jin Zhang (Member, IEEE) received the bachelor's and master's degrees from the Department of Electronic Engineering, Tsinghua University, Beijing, China, in 2004 and 2006, respectively, and the Ph.D. degree from the Department of Computer Science and Engineering, Hong Kong University of Science and Technology, Hong Kong.

She is currently an Assistant Professor with the Computer Science and Engineering Department, Southern University of Science and Technology, Shenzhen, China. Her research interests are mainly in next-generation wireless networks, network economics, mobile computing in healthcare, cooperative communication, and networks.

Qian Zhang (Fellow, IEEE) received the B.S., M.S., and Ph.D. degrees in computer science from Wuhan University, Wuhan, China, in 1994, 1996, and 1999, respectively.

She was with Microsoft Research Asia, Beijing, China, in July 1999, where she was the Research Manager with the Wireless and Networking Group. In September 2005, she joined Hong Kong University of Science and Technology, Hong Kong, where she is a Full Professor with the Department of Computer Science and Engineering. She has published about 300 refereed papers in international leading journals and key conferences in the areas of wireless/Internet multimedia networking, wireless communications and networking, wireless sensor networks, and overlay networking.

Prof. Zhang has received the MIT TR100 (MIT Technology Review) World's Top Young Innovator Award and the Best Asia–Pacific Young Researcher Award elected by the IEEE Communication Society in 2004. She is a Fellow of IEEE for his contribution to the mobility and spectrum management of wireless networks and mobile communications.